

Cool molecular highly charged ions for precision tests of fundamental physics

Carsten Zülch,¹ Konstantin Gaul,^{1,*} Steffen M. Giesen,¹ Ronald F. Garcia Ruiz,^{2,3} and Robert Berger^{1,3,†}

¹*Fachbereich Chemie, Philipps-Universität Marburg,
Hans-Meerwein-Straße 4, 35032 Marburg, Germany*

²*Massachusetts Institute of Technology, Cambridge, MA 02139, USA*

³*CERN, CH-1211 Geneva 23, Switzerland*

(Dated: March 22, 2022)

Molecules and atomic highly charged ions provide powerful low-energy probes of the fundamental laws of physics: Polar molecules possess internal fields suitable to enhance fundamental symmetry violation by several orders of magnitudes, whereas atoms in high charge states can feature large relativistic effects and compressed level structures, ideally posed for high sensitivity to variations of fundamental constants. Polar, highly charged molecules could benefit from both: large internal fields and large relativistic effects. However, a high charge dramatically weakens chemical bonding and drives systems to the edge of Coulomb explosion. Herein, we propose multiply-charged polar molecules, that contain actinides, as promising candidates for precision tests of physics beyond the standard model. Explicitly, we predict PaF^{3+} to be thermodynamically stable, coolable and well-suited for precision spectroscopy. The proposed class of compounds, especially with short-lived actinide isotopes from the territory of pear-shaped nuclei, has potential to advance our understanding of molecules under extreme conditions, to provide a window into unknown properties of atomic nuclei, and to boost developments in molecular precision spectroscopy in various areas, such as optical clocks and searches for new physics.

As of today, important aspects of our universe are hardly understood, such as the nature of dark matter [1] and the origin of the imbalance between matter and anti-matter [2]. Thus, theories that go beyond the current standard model of particle physics are invoked, usually referred to as new physics. Such new physics introduces additional sources of symmetry violations, like the simultaneous violations of the symmetries with respect to spatial inversion (known as parity P) and of the relative direction of time (known as time-reversal T) [3]. Polar, heavy-elemental molecules like ThO allow currently some of the most precise low-energy tests of P, T -violation [4] as they are easy to polarize and possess large internal fields that enhance effects of new physics by several orders of magnitude compared to atoms [5]. Complementary opportunities to probe new physics are offered by atomic

highly charged ions (HCIs) [6]. In these systems the electronic spectra are often compressed due to the deshielded nuclear charge which results in energetically close-lying levels as well as large relativistic effects. This special electronic structure can for instance provide favourable enhancement of hypothetical spatio-temporal variations of the fine structure constant [7] by several orders of magnitude [8]. In contrast to neutral systems, HCIs can be trapped comparatively easily in deep potential wells and cooled by different mechanisms such as sympathetic cooling [9, 10] with well understood atomic ions such as Be^+ , paving the way to high-precision experiments and additionally to direct laser-cooling [6].

Small polar molecular HCIs (PMHCI) can combine advantages of polar molecules and atomic HCIs. In addition to the unification of large relativistic effects of HCIs with large internal fields of polar molecules, as HCIs the PMHCIs could induce a transition from Madelung to Coulomb ordering of electronic levels. Coulomb ordered levels could pave the way for first direct laser-cooling of a molecular ion, as until now laser-cooling of molecular ions was limited due to unfavorable arrangement of electronic states compared to neutral molecules [11, 12]. However, several hurdles have to be overcome: i) Few *stable* and *meta-stable* small molecules with charge number larger than two are known [13, 14]. Most long-lived *meta-stable* triply and quadruply charged polar diatomic molecules, which were proposed theoretically or observed experimentally, are fluorides, oxides or noble gas compounds of metals [13, 14]. But only one *stable* triply charged polar diatomic molecule, UF^{3+} , is experimentally confirmed as of yet [15]. The difficulty lies in the requirement of very stable bonds that are able to counter the large electrostatic repulsion of two or more positive charges that usually lead to spontaneous Coulomb explosion. ii) Heavy-elemental molecules are preferred for the search for new physics, which severely limits the choice of possible systems, as P, T -violating effects are relativistic in nature and scale steeply with increasing nuclear charge Z [16]. Moreover, actinide nuclei such as Pa ($Z = 91$) are predicted to enhance the sensitivity to P, T -violating nuclear properties by up to 5 orders of magnitude when compared to molecules with stable nuclei [17]. iii) For precision spectroscopy, it is essential to cool and per-

fectly control the molecule. iv) And finally a simple electronic structure is desired to minimize systematic effects.

In this article we demonstrate that a variety of small PMHCIs suitable for precision tests of fundamental physics exist and propose PaF^{3+} as a promising candidate. We show its stability with respect to Coulomb explosion, characterize its electronic levels, propose how to cool it for precision spectroscopy, and compute its sensitivity to new physics. Moreover, we point out further possibly stable highly charged molecules and anticipate the impact that our results will have on molecular precision experiments in future.

The stability of a triply charged molecule AX^{3+} can be deduced from a simple rule of thumb [13, 18]: The third ionization energy $E_i(\text{A}^{2+})$ of atom A should be lower or at least nearly equal to the first ionization energy $E_i(\text{X})$ of atom X. Indeed, the third ionization energies of the first five actinides (Ac, Th, Pa, U and Np) are low compared to those of other elements (< 20 eV) [19–21]. The first ionization energies of neon (21.564 eV), fluorine (17.4 eV) [22] oxygen (13.6 eV) and nitrogen (14.5 eV) are relatively large in comparison [22–24]. Whereas trications with rare gas atoms such as CNe^{3+} have been considered theoretically early on by Koch and Frenking [25], corresponding bond dissociation energies are comparatively low. Instead, we expect actinide fluorides to be most stable followed by nitrides and oxides. UF^{3+} was already shown to be stable [15], but it has two unpaired f-electrons, which may complicate the extraction of fundamental parameters from precision spectroscopy experiments. As uranium has a higher ionization energy than Ac, Th and Pa we can expect that the molecules AcF^{3+} , ThF^{3+} and PaF^{3+} are stable as well. In the following we focus on PaF^{3+} as this molecule is isoelectronic to RaF , which has a comparatively simple electronic structure and is known to be well suited for the study of fundamental physics [26–29]. Moreover, the isotope ^{229}Pa attained much attraction as it is supposed to possess an extraordinary large static octupole deformation [30–32], which would render ^{229}Pa highly powerful for the search for P, T -violations in the quark-sector [33, 34]. Until now, experimental knowledge of Pa isotopes is scarce, and molecules containing Pa isotopes are promising systems to access electroweak properties of Pa nuclei. To our knowledge no molecule containing ^{229}Pa that is suitable for precision spectroscopy was proposed so far. Here, we show that PaF^{3+} offers a versatile laboratory for precision studies of fundamental physics.

We study the stability of PaF^{3+} with respect to the dissociation into $\text{Pa}^{2+} + \text{F}^+$, $\text{Pa}^{3+} + \text{F}$ and $\text{Pa}^{4+} + \text{F}^-$ with state-of-the-art coupled cluster calculations and quasirelativistic density functional theory. The charge separation dissociation channel $\text{Pa}^{2+} + \text{F}^+$ is at 4.1 eV, whereas the dissociation channels $\text{Pa}^{3+} + \text{F}$ and $\text{Pa}^{4+} + \text{F}^-$ lie above this at 4.9 eV and 32.1 eV, respectively. More details can be found in the methods section. An overview of

the dissociation channels of PaF^{3+} and PaF^{4+} is shown in Fig. 1B and in Tables I to III. We can conclude that PaF^{3+} is very stable. Crude estimates of the repulsive potential for $\text{Pa}^{3+} + \text{F}^+$ suggest that even PaF^{4+} could be meta-stable, i.e. the charge separation channel lies below the ground state potential but the potentials cross far from equilibrium, with a dissociation barrier > 1 eV (see methods section for details).

We computed vertical excitation energies, equilibrium bond lengths and harmonic vibrational wavenumbers of PaF^{3+} on the level of Dirac–Coulomb Fock-Space Coupled Cluster with Singles and Doubles amplitudes (DC-FSCCSD) and within a Zeroth Order Regular Approximation complex Generalized Hartree-Fock (ZORA-cGHF) self consistent field maximum overlap approach. With the ZORA-cGHF approach we determine transition electric dipole moments, projection of the orbital angular momentum on the molecular axis and hyperfine coupling constants, here reported for $^{231}\text{PaF}^{3+}$, as nuclear magnetic dipole moments for other Pa isotopes are lacking. ZORA-cGHF calculations can be assumed to be accurate within about 10% in comparison to FSCCSD calculations. And effects of larger basis sets are on the order of 5% (for details see the methods section and Table IV).

All electronic states explicitly studied herein are below the lowest dissociation channel at 4.1 eV (see Fig. 2 on the left and Table IV; potential curves at other levels of theory are provided in Supplementary Figures S1 – S5). A short bond length of about 1.85 Å and a large harmonic vibrational wavenumber ~ 850 cm^{-1} indicate a strong Pa–F bond. The level of mixing due to spin-orbit coupling is estimated from the projection of the orbital angular momentum on the molecular axis Λ . We find that the $(X)5/2$ ground state is of 90% Φ and 10% Δ character and the first two excited states are of 80% Δ and 20% Π character [(1)3/2 state] and 60% Π and 40% Σ character [(1)1/2 state], respectively. As can be seen in Fig. 2 on the left all electronic states of PaF^{3+} appear to have almost parallel potential curves, with bond lengths and harmonic vibrational wavenumbers varying less than 5%. This indicates that electronic excitations are determined by transitions between non-bonding spinors or spinors with nearly the same bonding or anti-bonding character. To characterize the involved atomic orbitals we compare the complex singly occupied ZORA-cGHF spinor to the large component of the analytic solution of the Dirac equation for the hydrogen atom for principal quantum number $n = 5$ (see Fig. 2 on the right). This confirms that the excited states are dominated by single-electron transitions between non-bonding or weakly anti-bonding orbitals. The seven lowest states are dominated by a singly occupied f-orbital located at Pa, of which the three lowest electronic states are characterized by a $5f_{5/2}$ orbital, and the next four states are characterized by a $5f_{7/2}$ orbital.

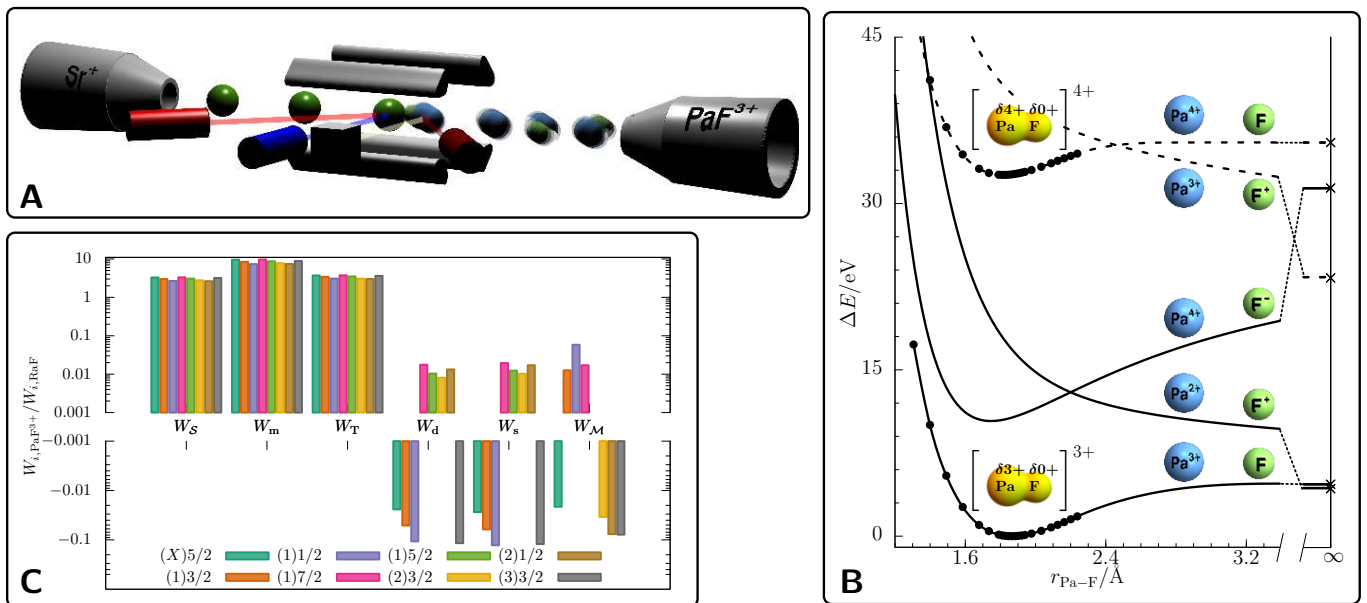


FIG. 1. Schematics of a search for P,T -violation in the quark-sector with the stable highly charged molecule PaF^{3+} . (A) Sketch of an experimental set-up for precision spectroscopy with PaF^{3+} . A decelerated beam of PaF^{3+} is trapped in a Paul trap, sympathetically cooled by Sr^+ ions and probed by the dark red laser. Further lasers for a potential direct cooling of the molecular ion PaF^{3+} are omitted for clarity. (B) Sketch of dissociation channels of PaF^{3+} (solid lines) and PaF^{4+} (dashed lines) as diabatic potentials. Ground state electronic potentials of PaF^{3+} and PaF^{4+} are shown as a spline interpolation of points computed at the level of ZORA-cGKS-PBE0, indicated as circles (molecular calculations) and crosses (separate atomic calculations). Potential curves for the repulsive channels $\text{Pa}^{2+} + \text{F}^+$ and $\text{Pa}^{3+} + \text{F}^+$ as well as the attractive channel $\text{Pa}^{4+} + \text{F}^-$ are represented with the model described in the methods section. Total electronic densities and Mulliken partial charges computed at the level of ZORA-cGKS-PBE0 are shown for the electronic ground states. (C) The parameters of the P,T -odd spin-rotational Hamiltonian of PaF^{3+} at the level of ZORA-cGHF relative to those of RaF computed in Ref. [35] scaled by $6/1.16$ (for details see the methods section).

The lowest six transition energies are narrowly spaced and squared transition electric dipole moments $|\bar{\mu}|^2$ indicate low transition rates. This is in accordance with electronic transitions involving primarily f-type atomic orbitals. Einstein coefficients for spontaneous emission roughly estimated from $|\bar{\mu}|^2$ and T_e at the level of ZORA-cGHF considering only electronic degrees of freedom are provided in Table V. From these we infer that the radiative lifetimes of the three lowest electronically excited states $[(1)3/2, (1)1/2, (1)7/2]$ could be on the order of ms, which is on the same order as the lifetime of the $H^3\Delta_1$ state in ThO that was used to provide the so far tightest upper bounds on molecular P,T -violation [4]. PaF^{3+} can be trapped and, due to a mass to charge ratio of about 83 u/e, efficiently cooled sympathetically with Sr^+ ions as sketched in Fig. 1A. Moreover, other cooling schemes, for instance with buffer gases, can be considered. In addition we find almost diagonal Franck-Condon matrices for all electronic transitions (see Table V) because of the non-bonding or weakly anti-bonding character of the highest occupied spinor and consequently almost parallel potential curves. When combined with an efficient pre-cooling scheme, direct laser-cooling of PaF^{3+} seems feasible. For instance the $(1)7/2 \leftarrow (X)5/2$ tran-

sition, which is at about 1800 nm has an estimated cumulated Franck-Condon factor of 0.999997 when taking the 0-0, 1-0 vibrational transitions into account on this level of theory and an estimated lifetime of < 20 ms. Another possibility for direct laser-cooling could be a population of the meta-stable $(1)1/2$ -state and cycling in the $(2)1/2 \leftarrow (1)1/2$ transition at about 1800 nm, which has a similar estimated Franck-Condon factor (0.999992) but a probably much shorter lifetime (< 70 μs). These properties clearly point to favourable prospects to obtain cold samples of PaF^{3+} for precision experiments.

In order to estimate the enhancement of new physics effects in PaF^{3+} we compute the electronic structure parameters W_i of the P,T -violating spin-rotational Hamiltonian [35–37] that reads in good approximation (see methods section for details)

$$H_{\text{sr}} = \Omega (W_d d_e + W_s k_s) + \Theta W_M \tilde{\mathcal{M}} + \mathcal{I} (W_T k_T + W_S \mathcal{S} + (W_m + W_S R_{\text{vol}}) d_p), \quad (1)$$

where Ω is the projection of the total electronic angular momentum on the molecular axis, \mathcal{I} is the projection of total spin of Pa on the molecular axis and Θ accounts for the electron and nuclear spin interaction along the molecular axis [35, 37]. We account here for

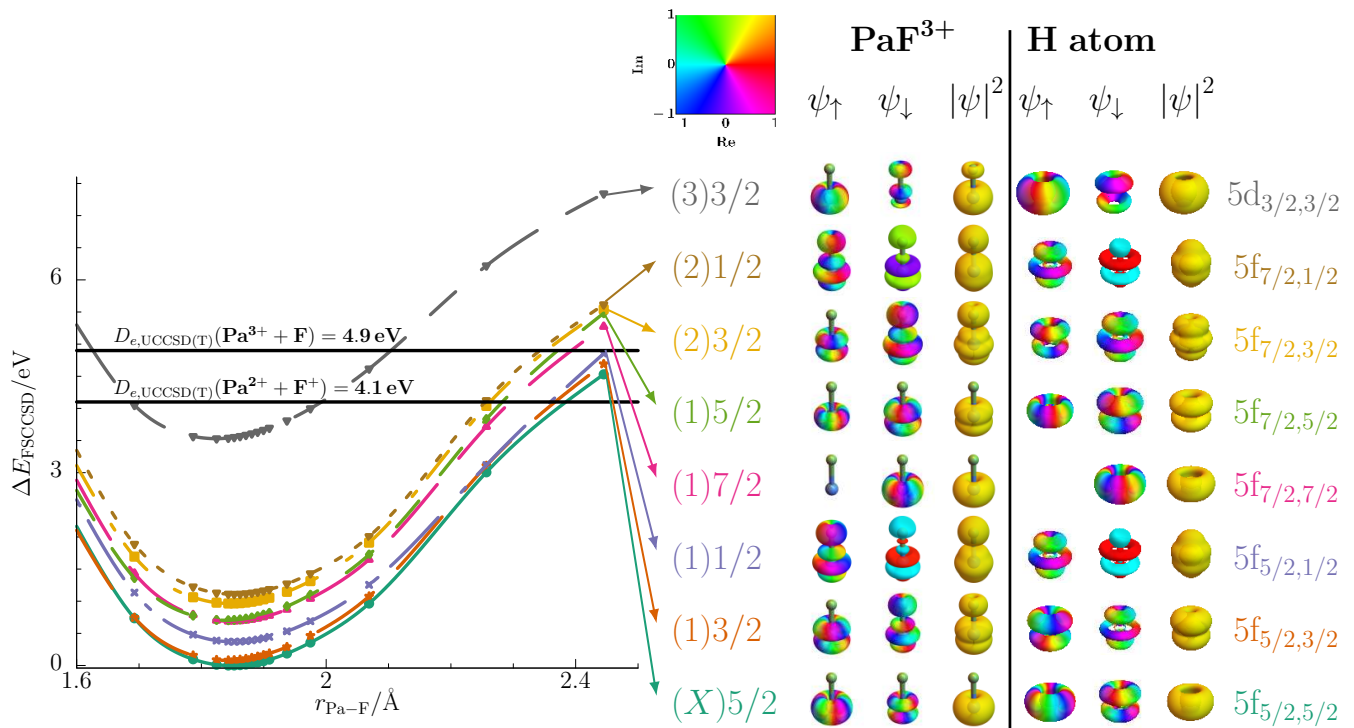


FIG. 2. Potential energy curves for the eight energetically lowest electronic states relative to the ground state of PaF^{3+} computed at the level of DC-FSCCD/ANO-RCC. Lines between the points are shown to guide the eye. The two lowest dissociation channels $\text{Pa}^{2+} + \text{F}^+$ and $\text{Pa}^{3+} + \text{F}$, as computed on a higher level of theory (RECP-UCCSD(T)-SOC), are indicated by black horizontal lines. The various electronic states are additionally characterized by the complex two-component ZORA-cGHF spinor $\psi = (\psi_\uparrow, \psi_\downarrow)$ of the unpaired electron and compared to the upper component of the analytic solution of the Dirac equation for the hydrogen atom. Atomic hydrogen spinors are labelled as ℓ_{j,m_j} , where ℓ is the symbol for the electronic orbital angular momentum quantum number, j is the total electronic angular momentum quantum number and m_j is the magnetic total electronic angular momentum quantum number.

P, T -violation in a molecule via an electric dipole moment of the electron d_e , an electric dipole moment of the proton d_p , the collective Schiff moment \mathcal{S} , the nuclear magnetic quadrupole moment \mathcal{M} , the P, T -odd scalar-pseudoscalar nucleon-electron current k_s , and tensor-pseudotensor nucleon-electron current k_T interactions. R_{vol} is a nuclear structure factor. *Ab initio* results for the various W_i parameters at the level ZORA-cGHF for the eight lowest electronic states of PaF^{3+} are provided in Table VI and are compared to the isoelectronic RaF molecule in Fig. 1C. The large enhancement of P, T -odd effects that stem from P, T -violation in the quark-sector. In the $X(5/2)$ state the collective Schiff moment is enhanced by $W_{\mathcal{S}} \sim -72\,000 e/(4\pi\epsilon_0)/a_0^4$, which is more than three times larger in absolute value than in isoelectronic RaF ($\sim -21\,000 e/(4\pi\epsilon_0)/a_0^4$ computed with the same method [35]). We analyse this large absolute value of $W_{\mathcal{S}}$ in comparison to RaF in Fig. 3. Whereas in RaF the singly occupied molecular orbital (SOMO) has a pronounced s-character, with its contribution to $W_{\mathcal{S}}$ partially cancelling the contribution from the highest doubly occupied orbital (SOMO-1), there is no contribution from the f-type SOMO in PaF^{3+} . Furthermore, we see an

additive uncompensated contribution from the core orbitals in PaF^{3+} and a much larger contribution from the (SOMO-1), which can be attributed to the pronounced relativistic effects in PaF^{3+} . Similar effects are observed for the enhancement factors W_T and W_m . Thereby, the magnetic interaction with a valence proton W_m is up to ten times larger than in RaF . We can thus conclude that PaF^{3+} has a pronounced sensitivity to P, T -violation in the quark-sector.

Atomic f-type orbitals, which determine essentially the SOMO of PaF^{3+} , have vanishing probability density within the nucleus, so that P, T -odd effects dependent on the electron spin (W_d, W_s) are suppressed. However, in the possibly meta-stable (1)1/2-state, these effects are still on the same order as in BaF , for which an experiment to search for d_e is planned [38]. The relative suppression of electron-spin dependent effects can be an advantage for the disentanglement of the fundamental sources of P, T -violation, for which the ratio of different enhancement factors W_i plays an important role [17, 39]. The ratio of W_d/W_s is 12% lower than predicted by the model presented in Ref. [39] for $Z = 91$ and, thus, would correspond to $Z = 97$ in the model. This can be ex-

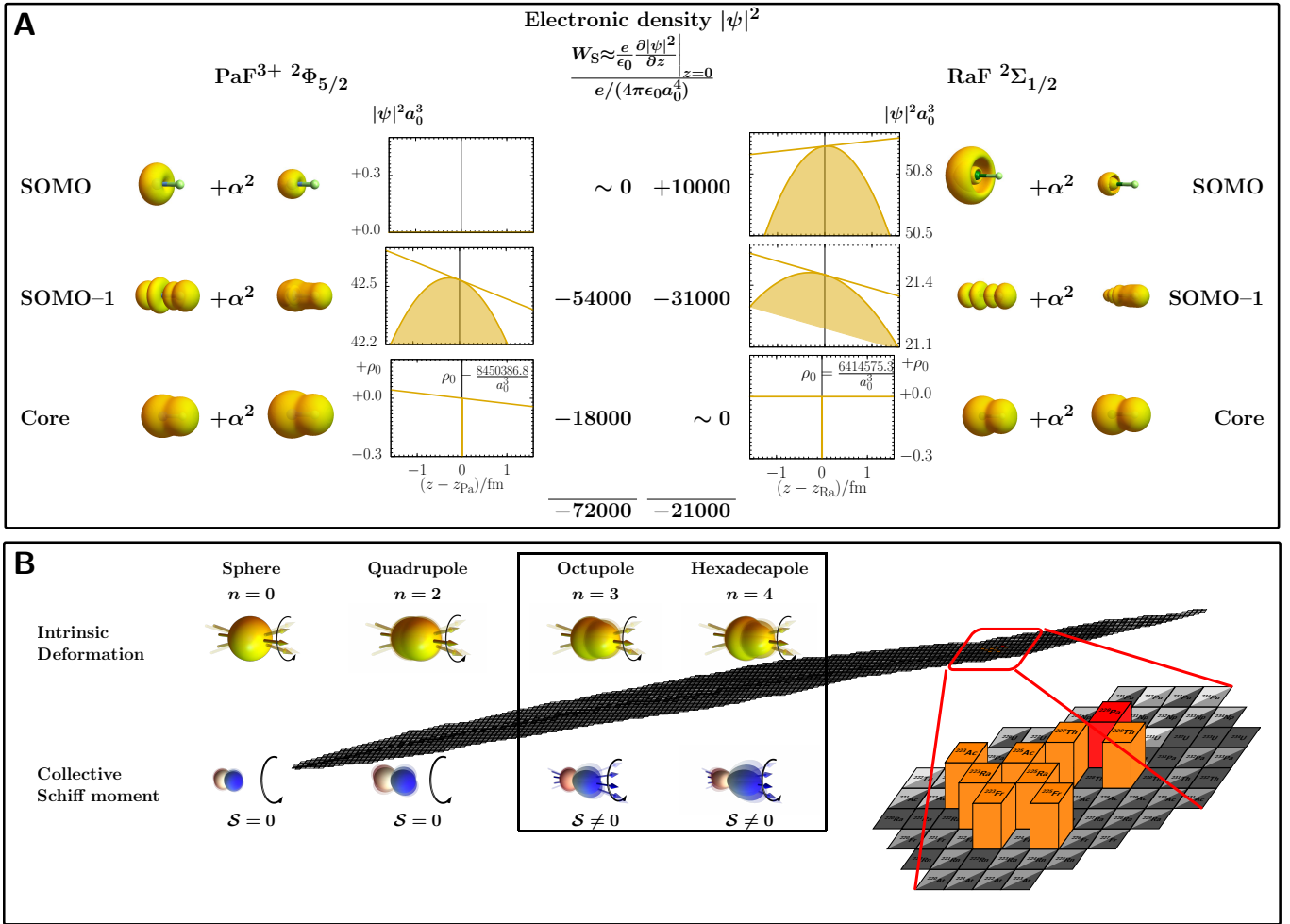


FIG. 3. Visualization of enhancement of P, T -violation in the quark-sector within the PMHCI PaF³⁺ compared to isoelectronic RaF, illustrated by example of the nuclear Schiff moment. This moment would induce an energy shift proportional to $S W_S \mathcal{I}$ (see text). (A) Enhancement as per the electronic structure parameter W_S is shown. Non-vanishing W_S stems from a shift of the maximum electron density away from the nuclear center by polarization, which in good approximation is characterized by the slope of the four-component (4c) electron density (indicated by a line in the middle) at the position of the Pa or Ra nucleus. Contributions from the SOMO, the highest doubly occupied orbital (SOMO-1) and uncompensated contributions from core electrons are shown. Approximate 4c electron densities computed at the ZORA-cGHF level are plotted with contour value of $0.035^2 a_0^{-3}$, with lower component density contributions (right isodensities) being magnified by α^{-2} to enhance visibility as compared to the upper component (left isodensities). In each isodensity plot, the heavy nucleus (Pa, Ra) is located on the left, the fluorine nucleus on the right as indicated by the ball-and-stick structures. (B) Visualization of the strong enhancement of a collective Schiff moment S in octupole deformed nuclei. Large octupole deformations accumulate in the highlighted region of the nuclide chart. Nuclear charge densities with deformation of order n and corresponding angular densities of the Schiff operator are modeled in spherical plots (for details on how this is realized see the methods section). The resulting collective Schiff moments S are indicated by a vector of length S along the deformation axis in the intrinsic frame. The precession of the intrinsic moment around the z -axis is also indicated.

plained by the high charge of the molecule that leads to a higher effective nuclear charge. The ratios between other parameters are considerably different compared to RaF and some even have opposite sign. All this renders experiments with PaF³⁺ complementary in the search for P, T -violation to other experiments with polar open-shell molecules.

Moreover, PaF³⁺ can also be advantageous for other tests of fundamental physics. The electronic potentials of

PaF³⁺ are largely overlapping, leading to possibly very close lying nearly degenerate vibrational states. In combination with the large relativistic effects this could result in a high sensitivity to a variation of fundamental constants [40].

In summary, highly charged polar actinide molecules can be stable and have favourable properties for precision tests of fundamental physics. Such PMHCIs can be cooled sympathetically and can show a pronounced

enhancement of new physics effects in the quark-sector. In particular, we demonstrated that the molecule PaF^{3+} is favorable for precision tests of fundamental physics. PaF^{3+} has a very simple electronic structure with one valence f-electron in a non-bonding or weakly anti-bonding orbital located at Pa. This leads to parallel potential curves for essentially all energetically low-lying electronic states, which may allow to establish an efficient direct laser-cooling scheme after sympathetic pre-cooling with Sr^+ ions or pre-cooling in a buffer-gas cell. Furthermore, due to the high charge many close lying states can be found that may be advantageous in the search for a variation of fundamental constants.

Beyond PaF^{3+} , we suggest to study also the PMHCIs UO^{3+} and NpN^{3+} as possibly stable candidates for molecular precision spectroscopy. From the discussion above we infer, moreover, that ThF^{3+} can be a very stable closed-shell highly charged molecule. Furthermore, doubly charged molecular ions, such as ThF^{2+} and PaO^{2+} that are isoelectronic to RaF , might also be considered for high-precision spectroscopy. Some selected molecular properties computed for PaO^{2+} are reported in Table S6-S8 in the Supplementary Material. Previously, PaO^{2+} was studied theoretically [41] and observed in the gas-phase [42]. From this it can be expected that PaO^{2+} has similar properties as PaF^{3+} . Sympathetic cooling or pre-cooling of these doubly charged ions may be achievable with Ba^+ ions.

Recent progress [43–45] allows precision searches for new physics with polyatomic molecules and polyatomic molecular ions which provide several experimental benefits [46, 47]. We indicate here for instance PaNC^{3+} , PaNCS^{3+} as candidates for possibly stable polyatomic PMHCIs. Following Ref. [48] it may be worthwhile to study $[\text{PaNCCH}_3]^{4+}$ as potentially long-lived meta-stable symmetric-top PMHCI for a precision search for new physics.

Our study opens up a new route to molecular precision spectroscopy and is a starting point to search for further candidates of molecular HCIs. We anticipate that this class of systems has possible applications as optical clocks, for quantum logic spectroscopy and for precision test of new physics. Molecular HCIs such as PaF^{3+} advance our understanding of chemical bonding, can provide a powerful probe of nuclear electroweak properties and will boost precision searches for new physics beyond the standard model. These studies provide further motivation for the emergent field of short-lived radioactive molecules. This is timely with the development of future radioactive beam facilities such as the Facility for Rare Isotopes (FRIB) in the U.S., which starts operation in 2022, and is expected to produce unprecedented amounts of Pa isotopes and other actinide nuclei.

Acknowledgments.—We thank Nicholas R. Hutzler, Andrei Zaitsevskii and Timur Isaev for discussions and Gernot Frenking for his comments on the manuscript.

R.B. is indebted to Helmut Schwarz, Jana Roithova and the late Detlef Schröder for early discussions on highly charged molecular ions. This work was funded by the Deutsche Forschungsgemeinschaft (DFG, German Research Foundation) – Projektnummer 445296313. Computer time provided by the center for scientific computing (CSC) Frankfurt is gratefully acknowledged.

Author contributions.—R.F.G.R. had the initial idea to search for a Pa containing molecule for tests of fundamental physics. K.G. and R.B. proposed PaF^{3+} as possible candidate molecule and coordinated the research project. K.G. did preliminary calculations on the stability of PaF^{3+} and its symmetry violating properties and implemented the MOM scheme for quasi-relativistic calculations of excited states. S.M.G. provided an implementation for matrix elements of non-orthogonal wave function and for visualization of complex two-component orbitals. C.Z. did all calculations presented in the final version of the manuscript. C.Z. and K.G. wrote the initial draft of the manuscript. All authors contributed to the discussion and the final version of the manuscript.

Extended Data.—Explicit numerical values for dissociation energies of PaF^{3+} and PaF^{4+} and ionization energies of Pa, F are given at different levels of theory. Spectroscopic constant of PaF^{3+} are provided at the two-component ZORA and FSCCSD levels of theory. Franck-Condon factors, Einstein coefficients and estimated lifetimes for the eight lowest states of PaF^{3+} are given at the level of ZORA-cGHF. Explicit values of P, T -odd properties for the eight lowest electronic states are given at the ZORA two-component level.

Supplementary information.—We provide the potential energy curves of selected electronic states of PaF^{3+} at different levels of theory and the potential energy curve of PaF^{4+} at the level of FSCCSD. Selected properties of PaO^{2+} for the lowest three electronic states are given at the level of ZORA-cGKS-B3LYP. We provide all data to reproduce the figures shown in the main text and the supplement.

-
- * konstantin.gaul@staff.uni-marburg.de; kongaul@web.de
 † robert.berger@uni-marburg.de
- [1] Spergel, D. N. The dark side of cosmology: Dark matter and dark energy. *Science* **347**, 1100–1102 (2015). URL <https://science.sciencemag.org/content/347/6226/1100>.
 - [2] Canetti, L., Drewes, M. & Shaposhnikov, M. Matter and antimatter in the universe. *New J. Phys.* **14**, 095012 (2012). URL <https://doi.org/10.1088%2F1367-2630%2F14%2F9%2F095012>.
 - [3] Gross, D. J. The role of symmetry in fundamental physics. *Proc. Natl. Acad. Sci. USA* **93**, 14256–14259 (1996). URL <http://www.pnas.org/content/93/25/14256.full>.
 - [4] Andreev, V. *et al.* Improved limit on the electric dipole

- moment of the electron. *Nature* **562**, 355–360 (2018). URL <https://doi.org/10.1038/s41586-018-0599-8>.
- [5] DeMille, D. Diatomic molecules, a window onto fundamental physics. *Physics Today* **68**, 34–40 (2015). URL <https://doi.org/10.1063/PT.3.3020>. <https://doi.org/10.1063/PT.3.3020>.
- [6] Kozlov, M. G., Safronova, M. S., Crespo López-Urrutia, J. R. & Schmidt, P. O. Highly charged ions: Optical clocks and applications in fundamental physics. *Rev. Mod. Phys.* **90**, 045005 (2018). URL <https://link.aps.org/doi/10.1103/RevModPhys.90.045005>.
- [7] Uzan, J.-P. The fundamental constants and their variation: observational and theoretical status. *Rev. Mod. Phys.* **75**, 403–455 (2003). URL <https://link.aps.org/doi/10.1103/RevModPhys.75.403>.
- [8] Berengut, J. C., Dzuba, V. A. & Flambaum, V. V. Enhanced laboratory sensitivity to variation of the fine-structure constant using highly charged ions. *Phys. Rev. Lett.* **105**, 120801 (2010). URL <https://link.aps.org/doi/10.1103/PhysRevLett.105.120801>.
- [9] Drewsen, M., Brodersen, C., Hornekær, L., Hangst, J. S. & Schiffrer, J. P. Large ion crystals in a linear paul trap. *Phys. Rev. Lett.* **81**, 2878–2881 (1998). URL <https://link.aps.org/doi/10.1103/PhysRevLett.81.2878>.
- [10] Bove, P. *et al.* Sympathetic crystallization of trapped ions. *Phys. Rev. Lett.* **82**, 2071–2074 (1999). URL <https://link.aps.org/doi/10.1103/PhysRevLett.82.2071>.
- [11] Nguyen, J. H. V. *et al.* Challenges of laser-cooling molecular ions. *New. J. Phys.* **13**, 063023 (2011). URL <https://doi.org/10.1088/1367-2630/13/6/063023>.
- [12] Ivanov, M. V., Jagau, T.-C., Zhu, G.-Z., Hudson, E. R. & Krylov, A. I. In search of molecular ions for optical cycling: a difficult road. *Phys. Chem. Chem. Phys.* **22**, 17075–17090 (2020). URL <http://dx.doi.org/10.1039/D0CP02921A>.
- [13] Schröder, D. & Schwarz, H. Generation, stability, and reactivity of small, multiply charged ions in the gas phase. *J. Phys. Chem. A* **103**, 7385–7394 (1999). URL <https://doi.org/10.1021/jp991332x>.
- [14] Franzreb, K. *et al.* Gas-phase diatomic trications of Se_2^{3+} , Te_2^{3+} , and LaF^{3+} . *J. Chem. Phys.* **121**, 12293–12302 (2004). URL <https://aip.scitation.org/doi/abs/10.1063/1.1821496>.
- [15] Schröder, D., Diefenbach, M., Klapötke, T. M. & Schwarz, H. UF^{3+} – a thermochemically stable diatomic trication with a covalent bond. *Angew. Chem. Int. Ed.* **38**, 137–140 (1999). URL <https://onlinelibrary.wiley.com/doi/abs/10.1002/%28SICI%291521-3773%2819990115%2938%3A1%2F3C137%3A%3AAID-ANIE137%3E3.O.CO%3B2-M>.
- [16] Khriplovich, I. B. & Lamoreaux, S. K. *CP Violation without Strangeness* (Springer, Berlin, 1997).
- [17] Chupp, T. E., Fierlinger, P., Ramsey-Musolf, M. J. & Singh, J. T. Electric dipole moments of atoms, molecules, nuclei, and particles. *Rev. Mod. Phys.* **91**, 015001 (2019). URL <https://link.aps.org/doi/10.1103/RevModPhys.91.015001>.
- [18] Bates, D. R. & Carson, T. R. Doubly charged diatomic molecular ions. *Proceedings of the Physical Society. Section A* **68**, 1199–1202 (1955). URL <https://doi.org/10.1088/0370-1298/68/12/417>.
- [19] Migdalek, J. & Glowacz-Proszkiewicz, A. Dirac–Fock + core-polarization calculations of E1 transitions in the francium isoelectronic sequence. *J. Phys. B* **40**, 4143–4154 (2007). URL <https://doi.org/10.1088/0953-4075/40/21/002>.
- [20] Wyart, J.-F. & Kaufman, V. Extended analysis of doubly ionized thorium (Th III). *Phys. Scr.* **24**, 941–952 (1981). URL <https://doi.org/10.1088/0031-8949/24/6/006>.
- [21] Cao, X. & Dolg, M. Theoretical prediction of the second to fourth actinide ionization potentials. *Mol. Phys.* **101**, 961–969 (2003). URL <https://doi.org/10.1080/0026897021000046807>. <https://doi.org/10.1080/0026897021000046807>.
- [22] Edlén, B. On the identification of Ar x and Ar xiv in the solar corona and the origin of the unidentified coronal lines. *Sol. Phys.* **9**, 439–445 (1969). URL <https://doi.org/10.1007/BF02391668>.
- [23] Eriksson, K. B. S. & Isberg, H. B. S. New measurements in the spectrum of atomic oxygen, O I. *Arkiv. Fysik* **24**, 549 (1963).
- [24] Eriksson, K. B. S. & Pettersson, J. E. New measurements in the spectrum of the neutral nitrogen atom. *Phys. Scr.* **3**, 211–217 (1971). URL <https://doi.org/10.1088/0031-8949/3/5/003>.
- [25] Koch, W. & Frenking, G. Theoretical investigations of small multiply charged cations. ii. CNe^{n+} ($1 \leq n \leq 4$). *J. Chem. Phys.* **86**, 5617–5624 (1987). URL <https://doi.org/10.1063/1.452538>.
- [26] Isaev, T. A., Hoekstra, S. & Berger, R. Laser-cooled RaF as a promising candidate to measure molecular parity violation. *Phys. Rev. A* **82**, 052521 (2010).
- [27] Isaev, T. A. & Berger, R. Lasercooled radium monofluoride: A molecular all-in-one probe for new physics. *ArXiv e-prints* **1302.5682**, physics.chem-ph (2013). URL <http://arxiv.org/abs/1302.5682>. 1302.5682.
- [28] Garcia Ruiz, R. F. *et al.* Spectroscopy of short-lived radioactive molecules. *Nature* **581**, 396–400 (2020). URL <https://doi.org/10.1038/s41586-020-2299-4>.
- [29] Udrescu, S. M. *et al.* Isotope shifts of radium monofluoride molecules. *Phys. Rev. Lett.* **127**, 033001 (2021). 2105.10549.
- [30] Ahmad, I., Gindler, J. E., Betts, R. R., Chasman, R. R. & Friedman, A. M. Possible ground-state octupole deformation in ^{229}Pa . *Phys. Rev. Lett.* **49**, 1758–1761 (1982). URL <https://link.aps.org/doi/10.1103/PhysRevLett.49.1758>.
- [31] Ahmad, I., Chasman, R. R., Greene, J. P., Kondev, F. G. & Zhu, S. Electron capture decay of 58-min $^{229}_{92}\text{U}$ and levels in $^{229}_{91}\text{Pa}$. *Phys. Rev. C* **92**, 024313 (2015). URL <https://link.aps.org/doi/10.1103/PhysRevC.92.024313>.
- [32] Singh, J. T. A new concept for searching for time-reversal symmetry violation using Pa-229 ions trapped in optical crystals. *Hyperfine Interact.* **240**, 29 (2019). URL <https://doi.org/10.1007/s10751-019-1573-z>.
- [33] Auerbach, N., Flambaum, V. V. & Spevak, V. Collective T- and P-odd electromagnetic moments in nuclei with octupole deformations. *Phys. Rev. Lett.* **76**, 4316–4319 (1996). URL <https://link.aps.org/doi/10.1103/PhysRevLett.76.4316>.
- [34] Flambaum, V. V. Enhanced nuclear Schiff moment and time-reversal violation in ^{229}Th -containing molecules. *Phys. Rev. C* **99**, 035501 (2019). URL <https://link.aps.org/doi/10.1103/PhysRevC.99.035501>.
- [35] Gaul, K. & Berger, R. Toolbox approach for quasi-relativistic calculation of molecular properties for precision tests of fundamental physics. *J. Chem. Phys.*

- 152**, 044101 (2020). URL <https://doi.org/10.1063/1.5121483>. 1907.10432.
- [36] Hinds, E. A. & Sandars, P. G. H. Electric dipole hyperfine structure of TlF. *Phys. Rev. A* **21**, 471–479 (1980). URL <https://link.aps.org/doi/10.1103/PhysRevA.21.471>.
- [37] Kozlov, M. G. & Labzowsky, L. N. Parity violation effects in diatomics. *J. Phys. B* **28**, 1933–1961 (1995).
- [38] Aggarwal, P. *et al.* Measuring the electric dipole moment of the electron in BaF. *Eur. Phys. J. D* **72**, 197 (2018). URL <https://doi.org/10.1140/epjd/e2018-90192-9>.
- [39] Gaul, K., Marquardt, S., Isaev, T. & Berger, R. Systematic study of relativistic and chemical enhancements of \mathcal{P} , \mathcal{T} -odd effects in polar diatomic radicals. *Phys. Rev. A* **99**, 032509 (2019). URL <https://link.aps.org/doi/10.1103/PhysRevA.99.032509>. 1805.05494.
- [40] Chin, C., Flambaum, V. V. & Kozlov, M. G. Ultracold molecules: new probes on the variation of fundamental constants. *New J. Phys.* **11**, 055048 (2009). URL <https://doi.org/10.1088/1367-2630/11/5/055048>.
- [41] Kovács, A., Infante, I. & Gagliardi, L. Theoretic study of the electronic spectra of neutral and cationic PaO and PaO₂. *Struct. Chem.* **24**, 917–925 (2013). URL <https://doi.org/10.1007/s11224-013-0251-z>.
- [42] Santos, M. *et al.* Oxidation of gas-phase protactinium ions, Pa⁺ and Pa²⁺: Formation and properties of PaO₂⁺(g), Protactinyl. *J. Phys. Chem. A* **110**, 5751–5759 (2006). URL <https://doi.org/10.1021/jp057297d>. PMID: 16640369, <https://doi.org/10.1021/jp057297d>.
- [43] Isaev, T. A. & Berger, R. Polyatomic candidates for cooling of molecules with lasers from simple theoretical concepts. *Phys. Rev. Lett.* **116**, 063006 (2016). URL <https://link.aps.org/doi/10.1103/PhysRevLett.116.063006>.
- [44] Kozyryev, I., Baum, L., Matsuda, K. & Doyle, J. M. Proposal for laser cooling of complex polyatomic molecules. *ChemPhysChem* **17**, 3641–3648 (2016). URL <https://onlinelibrary.wiley.com/doi/abs/10.1002/cphc.201601051>.
- [45] Fan, M. *et al.* Optical mass spectrometry of cold RaOH⁺ and RaOCH₃⁺. *Phys. Rev. Lett.* **126**, 023002 (2021). URL <https://link.aps.org/doi/10.1103/PhysRevLett.126.023002>.
- [46] Isaev, T. A., Zaitsevskii, A. V. & Eliav, E. Laser-coolable polyatomic molecules with heavy nuclei. *J. Phys. B* **50**, 225101 (2017). URL <http://stacks.iop.org/0953-4075/50/i=22/a=225101>.
- [47] Kozyryev, I. & Hutzler, N. R. Precision measurement of time-reversal symmetry violation with laser-cooled polyatomic molecules. *Phys. Rev. Lett.* **119**, 133002 (2017). URL <https://link.aps.org/doi/10.1103/PhysRevLett.119.133002>.
- [48] Harvey, J. N. & Kaczorowska, M. Microsolvation of metal ions: on the stability of [Zr(CH₃CN)]⁴⁺ and other multiply charged ions. *Int. J. Mass Spec.* **228**, 517–526 (2003). URL <https://www.sciencedirect.com/science/article/pii/S138738060300160X>. Special Issue: In honour of Helmut Schwarz.
- [49] DIRAC, a relativistic ab initio electronic structure program, Release DIRAC19 (2019), written by A. S. P. Gomes, T. Saue, L. Visscher, H. J. Aa. Jensen, and R. Bast, with contributions from I. A. Aucar, V. Bakken, K. G. Dyall, S. Dubillard, U. Ekström, E. Eliav, T. Enevoldsen, E. Faßhauer, T. Fleig, O. Fossgaard, L. Halbert, E. D. Hedegård, B. Heimlich–Paris, T. Helgaker, J. Henriksson, M. Iliaš, Ch. R. Jacob, S. Knecht, S. Komorovský, O. Kullie, J. K. Lærdahl, C. V. Larsen, Y. S. Lee, H. S. Nataraj, M. K. Nayak, P. Norman, G. Olejniczak, J. Olsen, J. M. H. Olsen, Y. C. Park, J. K. Pedersen, M. Pernpointner, R. di Remigio, K. Ruud, P. Salek, B. Schimmelpfennig, B. Senjean, A. Shee, J. Sikkema, A. J. Thorvaldsen, J. Thyssen, J. van Stralen, M. L. Vidal, S. Villaume, O. Visser, T. Winther, and S. Yamamoto (available at <http://dx.doi.org/10.5281/zenodo.3572669>, see also <http://www.diracprogram.org>).
- [50] Dyall, K. G. Relativistic and nonrelativistic finite nucleus optimized triple-zeta basis sets for the 4p, 5p and 6p elements. *Theor. Chem. Acc.* **108**, 335–340 (2002). URL <http://dx.doi.org/10.1007/s00214-002-0388-0>.
- [51] Dyall, K. G. Relativistic quadruple-zeta and revised triple-zeta and double-zeta basis sets for the 4p, 5p, and 6p elements. *Theor. Chem. Acc.* **115**, 441–447 (2006). URL <http://dx.doi.org/10.1007/s00214-006-0126-0>.
- [52] Roos, B. O., Lindh, R., Malmqvist, P., Veryazov, V. & Widmark, P.-O. New relativistic ANO basis sets for actinide atoms. *Chem. Phys. Lett.* **409**, 295–299 (2005). URL <https://www.sciencedirect.com/science/article/pii/S0009261405006810>.
- [53] van Wüllen, C. A Quasirelativistic Two-component Density Functional and Hartree-Fock Program. *Z. Phys. Chem* **224**, 413–426 (2010).
- [54] Ahlrichs, R., Bär, M., Häser, M., Horn, H. & Kölmel, C. Electronic structure calculations on workstation computers: The program system turbomole. *Chem. Phys. Lett.* **162**, 165–169 (1989).
- [55] van Wüllen, C. Molecular density functional calculations in the regular relativistic approximation: Method, application to coinage metal diatomics, hydrides, fluorides and chlorides, and comparison with first-order relativistic calculations. *J. Chem. Phys.* **109**, 392–399 (1998).
- [56] Liu, W., van Wüllen, C., Wang, F. & Li, L. Spectroscopic constants of MH and M₂ (M = Tl, E113, Bi, E115): direct comparisons of four- and two-component approaches in the framework of relativistic density functional theory. *J. Chem. Phys.* **116**, 3626–3634 (2002).
- [57] Vosko, S. H., Wilk, L. & Nuisar, M. Accurate spin-dependent electron liquid correlation energies for local spin density calculations: A critical analysis. *Can. J. Phys.* **58**, 1200–1211 (1980).
- [58] Becke, A. D. Density-functional exchange-energy approximation with correct asymptotic-behavior. *Phys. Rev. A* **38**, 3098–3100 (1988).
- [59] Lee, C., Yang, W. & Parr, R. G. Development of the Colle-Salvetti correlation-energy formula into a functional of the electron-density. *Phys. Rev. B* **37**, 785–789 (1988).
- [60] Stephens, P. J., Devlin, F. J., Chabalowski, C. F. & Frisch, M. J. Ab initio calculation of vibrational absorption and circular dichroism spectra using density functional force fields. *J. Phys. Chem.* **98**, 11623–11627 (1994).
- [61] Perdew, J. P., Burke, K. & Ernzerhof, M. Generalized gradient approximation made simple. *Phys. Rev. Lett.* **77**, 3865–3868 (1996).
- [62] Adamo, C. & Barone, V. Toward reliable density func-

- tional methods without adjustable parameters: The PBE0 model. *J. Chem. Phys.* **110**, 6158–6170 (1999). URL <https://doi.org/10.1063/1.478522>.
- [63] Roos, B. O., Lindh, R., Malmqvist, P., Veryazov, V. & Widmark, P. O. Main Group Atoms and Dimers Studied with a New Relativistic ANO Basis Set. *J. Phys. Chem. A* **108**, 2851–2858 (2004).
- [64] Gaul, K. & Berger, R. Zeroth order regular approximation approach to electric dipole moment interactions of the electron. *J. Chem. Phys.* **147**, 014109 (2017).
- [65] Visscher, L. & Dyall, K. G. Dirac-fock atomic electronic structure calculations using different nuclear charge distributions. *At. Data Nucl. Data Tables* **67**, 207–224 (1997).
- [66] Gilbert, A. T. B., Besley, N. A. & Gill, P. M. W. Self-consistent field calculations of excited states using the maximum overlap method (MOM). *J. Phys. Chem. A* **112**, 13164–13171 (2008). URL <https://doi.org/10.1021/jp801738f>. PMID: 18729344, <https://doi.org/10.1021/jp801738f>.
- [67] Barca, G. M. J., Gilbert, A. T. B. & Gill, P. M. W. Simple models for difficult electronic excitations. *J. Chem. Theo. Comp.* **14**, 1501–1509 (2018). URL <https://doi.org/10.1021/acs.jctc.7b00994>. PMID: 29444408, <https://doi.org/10.1021/acs.jctc.7b00994>.
- [68] Berger, R., Fischer, C. & Klessinger, M. Calculation of the vibronic fine structure in electronic spectra at higher temperatures. 1. benzene and pyrazine. *J. Phys. Chem. A* **102**, 7157–7167 (1998).
- [69] Jankowiak, H.-C., Stuber, J. L. & Berger, R. Vibronic transitions in large molecular systems: Rigorous prescreening conditions for Franck-Condon factors. *J. Chem. Phys.* **127**, 234101 (2007).
- [70] Huh, J. & Berger, R. Coherent state-based generating function approach for Franck-Condon transitions and beyond. In *SYMMETRIES IN SCIENCE XV*, vol. 380 of *J. Phys. Conf. Ser.* (2012). International Symposium on Symmetries in Science XV, Bregenz, AUSTRIA, JUL 31-AUG 05, 2011.
- [71] Huh, J., Neff, M., Rauhut, G. & Berger, R. Franck-Condon profiles in photodetachment-photoelectron spectra of HS_2^- and DS_2^- based on vibrational configuration interaction wavefunctions. *Mol. Phys.* **108**, 409 (2010).
- [72] Löwdin, P.-O. Quantum theory of many-particle systems .1. physical interpretations by means of density matrices, natural spin-orbitals, and convergence problems in the method of configurational interaction. *Phys. Rev.* **97**, 1474–1489 (1955).
- [73] Flambaum, V. V. & Ginges, J. S. M. Nuclear Schiff moment and time-invariance violation in atoms. *Phys. Rev. A* **65**, 032113 (2002). URL <https://link.aps.org/doi/10.1103/PhysRevA.65.032113>.
- [74] Flambaum, V. V., Dzuba, V. A. & Tran Tan, H. B. Time- and parity-violating effects of the nuclear schiff moment in molecules and solids. *Phys. Rev. A* **101**, 042501 (2020). URL <https://link.aps.org/doi/10.1103/PhysRevA.101.042501>.
- [75] Werner, H.-J., Knowles, P. J., Knizia, G., Manby, F. R. & Schütz, M. Molpro: a general-purpose quantum chemistry program package. *WIREs Computational Molecular Science* **2**, 242–253 (2012). URL <https://wires.onlinelibrary.wiley.com/doi/abs/10.1002/wcms.82>.
- [76] Werner, H.-J. *et al.* Molpro, version 2019.2, a package of ab initio programs (2019). See <http://www.molpro.net>.
- [77] Werner, H.-J. *et al.* The molpro quantum chemistry package. *J. Chem. Phys.* **152**, 144107 (2020). URL <https://doi.org/10.1063/5.0005081>.
- [78] Cao, X., Dolg, M. & Stoll, H. Valence basis sets for relativistic energy-consistent small-core actinide pseudopotentials. *J. Chem. Phys.* **118**, 487–496 (2003). URL <https://doi.org/10.1063/1.1521431>.
- [79] Dunning, T. H., Jr. Gaussian basis sets for use in correlated molecular calculations. i. the atoms boron through neon and hydrogen. *J. Chem. Phys.* **90**, 1007–1023 (1989).
- [80] Wolfram Research, Inc. Mathematica 11.0 (2016).
- [81] Batista, E. R., Martin, R. L. & Hay, P. J. Density functional investigations of the properties and thermochemistry of UF_n and UCl_n ($n = 1, \dots, 6$). *J. Chem. Phys.* **121**, 11104–11111 (2004). URL <https://aip.scitation.org/doi/abs/10.1063/1.1811607>. <https://aip.scitation.org/doi/pdf/10.1063/1.1811607>.
- [82] Blondel, C., Delsart, C. & Goldfarb, F. Electron spectrometry at the μev level and the electron affinities of si and f. *J. Phys. B: Atom. Mol. Opt. Phys.* **34**, L281–L288 (2001). URL <http://stacks.iop.org/0953-4075/34/i=9/a=101>.
- [83] Walker, N. R., Wright, R. R., Barran, P. E., Murrell, J. N. & Stace, A. J. Comparisons in the behavior of stable Copper(II), Silver(II), and Gold(II) complexes in the gas phase: Are there implications for condensed-phase chemistry? *J. Am. Chem. Soc.* **123**, 4223–4227 (2001). URL <https://doi.org/10.1021/ja003431q>. PMID: 11457187.
- [84] Axe, J. D., Stapleton, H. J. & Jeffries, C. D. Paramagnetic resonance hyperfine structure of tetravalent Pa^{231} in Cs_2ZrCl_6 . *Phys. Rev.* **121**, 1630–1637 (1961). URL <https://link.aps.org/doi/10.1103/PhysRev.121.1630>.

METHODS

Computational methods

Relativistic four component calculations were performed with the quantum chemistry program package DIRAC19 [49] employing the Dirac–Coulomb (DC) Hamiltonian. The four-component Dirac–Coulomb Hartree–Fock (DC-HF) method was used to describe the electronic structure of Fluorine and Protactinium in different electron configurations, with the open-shell situation being treated within the average-of-configuration framework (ORHF). Relativistic Fock-space coupled-cluster calculations with singles and doubles cluster amplitudes (DC-FSCCD) were performed starting from the PaF⁴⁺ closed-shell electronic ground state as reference wavefunction and attaching an additional electron. Seven electrons of F ($2s^22p^5$) and 19 electrons of Pa ($5d^{10}6s^26p^65f^1$) were explicitly included in the electron correlation treatment. Virtual spinors were considered up to an energy of $50 E_h$. In DC-ORHF and DC-FSCCD calculations we employed the Dyall all-electron triple zeta (Dyall-ae3z) basis set for the Pa and F atom [50, 51] or a triple zeta atomic natural orbital type basis set (ANO-RCC-VTZP) [52]. To assess the quality of the basis set, additional calculations were performed with the Dyall all-electron quadruple zeta (Dyall-ae4z) basis set [50, 51]. DC-ORHF spinors were optimized in a self-consistent manner until a change in the orbital gradient below $10^{-7}/a_0^{3/2}$ was reached.

Quasirelativistic two-component calculations were performed with a modified version [53] of the quantum chemistry program package TURBOMOLE [54] at the level of complex generalized Hartree-Fock (cGHF) and complex generalized Kohn-Sham (cGKS) density functional theory (DFT) within the zeroth order regular approximation (ZORA) employing a model potential to alleviate the gauge dependence of the ZORA Hamiltonian as proposed by van Wüllen [55]. The ZORA-model potential was employed with additional damping [56]. Calculations on the DFT level were performed with the hybrid Becke three parameter exchange functional and the Lee, Yang and Parr correlation functional (B3LYP) [57–60], as well as with the hybrid version of the Perdew, Burke, Ernzerhof functional (PBE0) [61, 62]. On this level of theory, a basis set consisting of 37s, 34p, 14d and 9f uncontracted Gaussian functions with the exponential coefficients α_i composed as an even-tempered series as $\alpha_i = a/b^{i-1}$; $i = 1, \dots, N$, where N is the number of functions, with $b = 2$ for s and p functions and $b = (5/2)^{1/25} \times 10^{2/5} \approx 2.6$ for d and f functions was used for Pa. The largest exponent coefficients a of the subsets are $2 \times 10^9 a_0^{-2}$ (s), $5 \times 10^8 a_0^{-2}$ (p), $13300.758 a_0^{-2}$ (d) and $751.8368350 a_0^{-2}$ (f). A decontracted atomic natural orbital basis set of double- ζ quality augmented with polarization valence ba-

sis functions (ANO-RCC-VDZP) [63] was used for the F atom. These basis sets have performed well in previous studies of P, T -violation in molecules [27, 39, 64].

In all relativistic or quasi-relativistic calculations, a normalized spherical Gaussian nuclear density distribution $\rho_A(\vec{r}) = \frac{\zeta_A^{3/2}}{\pi^{3/2}} e^{-\zeta_A |\vec{r} - \vec{r}_A|^2}$ with $\zeta_A = \frac{3}{2r_{\text{nuc},A}^2}$ and the root-mean-square radius $r_{\text{nuc},A}$ was used as a finite nucleus as suggested by Visscher and Dyall [65]. Isotopes ²³¹Pa and ¹⁹F were used to determine the size of the finite nucleus. An exception to this are calculations of the energy gradient within the ZORA-cGKS approach, which were performed assuming a pointlike nucleus instead.

At the level of cGKS and cGHF, excited state orbitals were obtained by SCF calculations choosing occupation numbers regarding to maximum overlap with the determinant of the initial guess (initial guess maximum overlap method, IMOM) [66, 67]. As initial guess we used the cGKS or cGHF determinant, that was found with occupation of energetically lowest spinors. If the change in the differential density with respect to the previous cycle was below $10^{-3}/a_0^{-3}$ the standard MOM was used, where occupation numbers are chosen with respect to maximum overlap with the determinant of the previous cycle [66].

Franck–Condon factors were obtained with the program package HOTFCHT [68–71] by calculating the harmonic force constants with the module NumForce within the modified version of Turbomole mentioned above.

Transition electric dipole moments $\vec{\mu}$ were computed for the independently obtained cGHF and cGKS determinants using Löwdin rules [72] for single-particle operator transition matrix elements between nonorthogonal single-determinantal initial wave function Φ_i and final wave function Φ_f

$$\vec{\mu} = \langle \Phi_f | \vec{r} | \Phi_i \rangle = \sum_{ij} \langle \psi_{f,i} | \vec{r} | \psi_{i,j} \rangle \text{adj}(\mathbf{S})_{ij} \quad (2)$$

with the molecular spinors ψ_i of the initial (i) and final (f) state, approximately described by a single Slater determinant, and the adjugate of the overlap matrix between the initial and final state determinant with elements $S_{ij} = \langle \psi_{f,i} | \psi_{i,j} \rangle$.

All other molecular properties were computed with the toolbox approach presented in Ref. [35]. We neglected magnetic and hyperfine coupling induced interactions of d_e and k_s as well as higher order P, T -odd nuclear moments and described the nuclei in the non-relativistic limit. For a definition of the various electronic structure factors W_i except for W_S we refer to Ref.35. We used here a different definition of W_S than in Ref.35 which includes a factor of 6. Furthermore, we employed a finite nucleus model for the calculation of the W_S operator [73], whereas in Ref.35 a point-like nuclear model was used:

$$\begin{aligned} W_S &= -4\pi k_{\text{es}} e \left\langle \Psi \left| \frac{\partial}{\partial z} \rho_A(\vec{r}) \right| \Psi \right\rangle \\ &= 8\zeta_A \pi k_{\text{es}} e \langle \Psi | (z - z_A) \rho_A(\vec{r}) | \Psi \rangle, \end{aligned} \quad (3)$$

where the electrostatic constant k_{es} is $\frac{1}{4\pi\epsilon_0}$ in SI units and ϵ_0 is the electric constant. The last equality applies only to the spherical Gaussian nuclear model used in this work. In opposite to the operator used in Ref.35 this operator can be evaluated in numerical integration within the toolbox approach. As suggested in Ref.74, for direct comparison to the present values computed with a finite nuclear model for PaF^{3+} , we scaled the corresponding values of W_S of RaF that were obtained with the operator for a pointlike nucleus in Ref.35 by a factor of 1/1.6.

Bond lengths were optimized to an energy change of less than $10^{-6} E_h$ as convergence criterion. The wavefunctions were optimized to a change in energy and spin-orbit coupling contribution of $10^{-11} E_h$ or better, with exception of the calculations with the ANO-RCC-VTZP basis set, which was optimized to a change in energy and spin-orbit coupling contribution of $10^{-9} E_h$.

Calculations in a non-relativistic framework using scalar relativistic ECPs (RECP), which are reported in Tables I-III, were performed with the quantum chemistry program package MOLPRO [75-77] on the level of restricted open-shell Hartree-Fock (ROHF), spin-unrestricted-Kohn-Sham (UKS) using the functionals B3LYP and PBE0 and on the level of unrestricted coupled-cluster with iterative singles and doubles amplitudes combined with perturbative triples amplitudes (UCCSD(T)). For Pa a relativistic energy-consistent small-core pseudopotential (ECP60) was used together with atomic natural valence basis set [78]. An augmented correlation-consistent polarized basis with quadruple- ζ quality (aug-cc-pVQZ) [79] was used on the F-atom. The bond length was optimized up to a change in energy of $10^{-6} E_h$. Self consistent field calculations were performed until a change in the gradient in respect to the orbital rotation lower than $10^{-13} E_h/a_0$ was reached.

The complex two-component orbitals are visualized by calculating orbital amplitudes on a three-dimensional grid and plotting them with the help of MATHEMATICA version 11 [80] by mapping the phase in the complex plane via a color code on the contour surface of the absolute value of the spinors.

Dissociation channels

We study the stability of PaF^{3+} with respect to the dissociation into $\text{Pa}^{2+} + \text{F}^+$, $\text{Pa}^{3+} + \text{F}$ and $\text{Pa}^{4+} + \text{F}^-$ by separate energy calculations of the atomic products and the corresponding molecular species at its equilibrium structure with state-of-the-art unrestricted coupled cluster calculations with single and double amplitudes and perturbative triples [UCCSD(T)], in which we account for scalar-relativistic effects by a relativistic effective core potential (RECP). We find that the charge separation dissociation channel $\text{Pa}^{2+} + \text{F}^+$ is

at 5.1 eV. The dissociation channels $\text{Pa}^{3+} + \text{F}$ and $\text{Pa}^{4+} + \text{F}^-$ lie above this at 5.8 eV and 32 eV, respectively. In these calculations spin-orbit coupling is, however, not accounted for. To quantify this effect, quasi-relativistic two-component complex generalized Kohn-Sham (ZORA-cGKS) calculations within zeroth order regular approximation are compared to relativistic effective core potential unrestricted Kohn-Sham calculations (RECP-UKS), using the PBE0 functional, which performed well in the computation of bond dissociation energies of uranium halides [81]. The size of the spin-orbit coupling contribution to the three dissociation channels is -1.0 eV, -0.9 eV and 0.1 eV, respectively, yielding the spin-orbit corrected [RECP-UCCSD(T)+SOC] dissociation energies of 4.1 eV, 4.9 eV and 32.1 eV, which are in good agreement with dissociation energies at the level of ZORA-cGKS-PBE0 (3.8 eV, 4.7 eV and 32.5 eV). The RECP-UCCSD(T)+SOC method is in good agreement with ionization energies of Pa computed in Ref.21 (deviations $< 5\%$) and experimental ionization energy and electron affinity [22, 82] of F (deviations $< 1\%$).

From *ab initio* calculations we find that the dissociation channel $\text{Pa}^{3+} + \text{F}^+$ is placed ~ 10 eV below the equilibrium energy of PaF^{4+} . A crude estimate for a repulsive potential $V(r)$ as a function of the internuclear separation r can be obtained from purely repulsive Coulomb and Pauli potentials [48, 83]. Assuming that the ionic radius r_0 is equal for charge separation and homolytic dissociation, we model the Pauli repulsion by a Lennard-Jones potential $C^{(12)}/(r+r_0)^{12} - C^{(6)}/(r+r_0)^6$ for a fixed dissociation energy (indicated by crosses in Fig. 1 on the right), which is fitted to the ground state potentials of PaF^{3+} and PaF^{4+} computed on the level of ZORA-cGKS-PBE0 as indicated by circles in Fig. 1 on the right to obtain $V(r) = \Delta E + q_1q_2/(4\pi\epsilon_0(r+r_0)) + C^{(12)}/(r+r_0)^{12}$. Here ΔE is received at the level of ZORA-cGKS-PBE0 as described above and q_1q_2 is determined by the charge of the fragments. The fit of the ground state potential of PaF^{3+} yields $r_0 = 1.55 \text{ \AA}$, $C^{(12)} = 1.2 \times 10^7 \text{ eV \AA}^{12}$ and $C^{(6)} = 1.5 \times 10^4 \text{ eV \AA}^6$. The fit of the ground state potential of PaF^{4+} yields $r_0 = 1.00 \text{ \AA}$, $C^{(12)} = 6.9 \times 10^5 \text{ eV \AA}^{12}$ and $C^{(6)} = 2.7 \times 10^3 \text{ eV \AA}^6$. Relative to the ground state energy of PaF^{3+} we receive for the $\text{Pa}^{2+} + \text{F}^+$ channel $\Delta E = 3.8 \text{ eV}$, $r_0 = 1.55 \text{ \AA}$, $C^{(12)} = 1.2 \times 10^7 \text{ eV \AA}^{12}$, $q_1q_2/(4\pi\epsilon_0) = 28.8 \text{ eV \AA}$ yielding an avoided crossing at $> 30 \text{ \AA}$ and for the $\text{Pa}^{3+} + \text{F}^+$ channel $\Delta E = 35.5 \text{ eV}$, $r_0 = 1.00 \text{ \AA}$, $C^{(12)} = 6.9 \times 10^5 \text{ eV \AA}^{12}$, $q_1q_2/(4\pi\epsilon_0) = 43.2 \text{ eV \AA}$ yielding an avoided crossing at $> 2.4 \text{ \AA}$ (see Fig. 1 right). This suggests that PaF^{4+} could be meta-stable with a dissociation barrier $> 1 \text{ eV}$. In this model the potential for the $\text{Pa}^{4+} + \text{F}^-$ channel is modeled as $V(r) = 32 \text{ eV} - 57.6 \text{ eV \AA}/(r + 1.55 \text{ \AA}) + 1.2 \times 10^7 \text{ eV \AA}^{12}/(r + 1.55 \text{ \AA})^{12} - 1.7 \times 10^4 \text{ eV \AA}^6/(r + 1.55 \text{ \AA})^6$.

In calculations of the dissociation energy (Table I) the

mean-field RECP-ROHF and ZORA-cGHF methods underestimate the dissociation energy dramatically as missing electron correlation destabilizes considerably the Fluoride ions (see also Table II). Moreover, in the ZORA-cGHF method spin-orbit coupling and spin-polarization are incorporated self-consistently. As both effects stabilize the Pa cations, the ZORA-cGHF values are much lower than those at correlated levels of theory due this imbalanced consideration of electron-correlation effects.

Electronic excitation energies

In calculations of the electronic spectra (Table IV) ZORA-cGHF results are in a good agreement with DC-FSCCSD results, with deviations in excitation wavenumbers of maximally 600 cm^{-1} (for higher excitations 1100 cm^{-1}) and deviations of harmonic vibrational wavenumbers and equilibrium bond lengths $\leq 10\%$. We expect other molecular properties at the level of ZORA-cGHF to be accurate within 10% . Furthermore, the effect of a larger basis set (ANO-RCC vs dyall.3aez vs dyall.4aez) in FSCCSD calculations is found to be $< 5\%$.

Visualisation of nuclear densities

Nuclear charge densities with deformation of order n visualised in Fig. 3 on the bottom are realised as spherical plots of a Rayleigh expansion with axial symmetry $R_n(\theta, \phi, r) = [1 + \sum_{l=2}^n a_l r^l Y_{l,0}(\theta, \phi)]$ averaged over the radial part as $\int R_n(\theta, \phi, r) \exp[-2/(3 \langle r^2 \rangle) r^2] r^2 dr$, with $a_2 = 0.231$, $a_3 = 0.097$, $a_4 = 0.04$ and $\langle r^2 \rangle = 1$. These coefficients are chosen for optimal representation and have no physical meaning. The Schiff moment operator can be written as $\hat{S} = (r^3 - 5/2 \langle r^2 \rangle r) Y_{10}(\theta, \phi)$. The corresponding Schiff moments are modeled in a spherical plot of the angular function $S(\theta, \phi) = \int \hat{S} R_n(\theta, \phi, r) \exp[-2/(3 \langle r^2 \rangle) r^2] r^2 dr$, with the resulting moment being calculated as $\mathcal{S} = \int S(\theta, \phi) \sin(\theta) d\theta d\phi$.

TABLE I. **Dissociation energies of PaF^{3+} given for the three most probable dissociation channels.** The dissociation channels correspond to $D_e(\text{A}^{n+} + \text{B}^{[+,0,-]}) = E(\text{A}^{n+}) + E(\text{B}^{[+,0,-]}) - E(\text{AB}^{[(n+1)+,n+,(n-1)+]})$.

| Method | $D_e(\text{Pa}^{2+} + \text{F}^+)/\text{eV}$ | $D_e(\text{Pa}^{3+} + \text{F})/\text{eV}$ | $D_e(\text{Pa}^{4+} + \text{F}^-)/\text{eV}$ |
|-------------------|--|--|--|
| RECP-ROHF | 2.7 | 4.2 | 30.8 |
| ZORA-cGHF* | 0.3 | 2.7 | 30.5 |
| RECP-UKS-B3LYP | 4.7 | 5.6 | 32.7 |
| ZORA-cGKS-B3LYP | 4.1 | 4.7 | 32.2 |
| RECP-UKS-PBE0 | 4.8 | 5.6 | 32.4 |
| ZORA-cGKS-PBE0 | 3.8 | 4.7 | 32.5 |
| RECP-UCCSD(T) | 5.1 | 5.8 | 32.0 |
| RECP-UCCSD(T)+SOC | 4.1 | 4.9 | 32.1 |

* The ZORA-cGHF method underestimates the dissociation energy dramatically (see discussion in the methods section).

TABLE II. **Relevant n -th ionization energies E_i and electron affinities E_{ea} for Pa and F in comparison with literature (lit) values.** Relative deviation is given as $\text{dev} = (\text{calculation} - \text{lit})/\text{lit}$.

| Method | $E_i(\text{Pa}^{2+})/\text{eV}$ | dev / % | $E_i(\text{Pa}^{3+})/\text{eV}$ | dev/% | $E_i(\text{F})/\text{eV}$ | dev/% | $E_{ea}(\text{F})/\text{eV}$ | dev/% |
|-------------------|---------------------------------|---------|---------------------------------|-------|---------------------------|-------|------------------------------|-------|
| RECP-ROHF | 17.2 | -8 | 27.9 | -10 | 15.7 | -10 | 1.31 | -64 |
| ZORA-cGHF | 18.0 | -4 | 29.1 | -6 | 15.6 | -10 | 1.27 | -63 |
| RECP-UKS-B3LYP | 18.4 | -2 | 30.3 | -2 | 17.5 | 0 | 3.24 | -5 |
| ZORA-cGKS-B3LYP | 18.4 | -1 | 31.1 | 1 | 17.8 | 2 | 3.67 | 8 |
| RECP-UKS-PBE0 | 18.4 | -1 | 30.2 | -2 | 17.6 | 1 | 3.43 | 1 |
| ZORA-cGKS-PBE0 | 18.4 | -1 | 31.1 | 1 | 17.4 | 0 | 3.40 | 0 |
| RECP-UCCSD(T) | 18.0 | -4 | 29.6 | -4 | 17.4 | -0 | 3.40 | 0 |
| RECP-UCCSD(T)+SOC | 18.0 | -3 | 30.5 | -1 | 17.4 | -0 | 3.40 | 0 |
| Literature | 18.7 ^a | — | 30.9 ^a | — | 17.4 ^b | — | 3.40 ^b | — |

^a Scalar relativistic effective core potential calculations at the level of complete active space self-consistent field (RECP-CASSCF) with a correction for spin-orbit coupling by comparison to multi-configuration Dirac-Hartree-Fock (MCDHF) calculations.[21]

^b Experimental data. $E_i(\text{F})/\text{eV}$ was measured in Ref.22 and $E_{ea}(\text{F})/\text{eV}$ was measured in Ref.82.

TABLE III. Dissociation energies for PaF^{4+} given for the two most probable dissociation channels as $D_e(\text{channel})$.

| Method | $D_e(\text{Pa}^{4+}+\text{F})/\text{eV}$ | $D_e(\text{Pa}^{3+}+\text{F}^+)/\text{eV}$ |
|-------------------|--|--|
| RECP-ROHF | 0.6 | -11.6 |
| ZORA-cGHF | 0.1 | -13.4 |
| RECP-UKS-B3LYP | 3.5 | -9.4 |
| ZORA-cGKS-B3LYP | 3.2 | -10.1 |
| RECP-UKS-PBE0 | 3.4 | -9.2 |
| ZORA-cGKS-PBE0 | 3.3 | -10.3 |
| RECP-UCCSD(T) | 3.7 | -8.6 |
| RECP-UCCSD(T)+SOC | 3.6 | -9.7 |

TABLE IV. **Spectroscopically relevant properties of the eight energetically lowest electronic states of PaF_3^+ .** Equilibrium bond length r_e , harmonic vibrational wavenumber $\tilde{\omega}_e$ and excitation wavenumber \tilde{T}_e estimated as vertical excitation energy are shown at the level of Dirac–Coulomb Fock-Space Coupled Cluster (DC-FSCCSD) with two different basis sets and at the level of Zeroth Order Regular Approximation complex Generalized Hartree-Fock (ZORA-cGHF). The projection of the electronic orbital angular momentum quantum number on the molecular axis Λ , the squared transition dipole moment $|\bar{\mu}|^2$ and hyperfine coupling constant along the molecular axis A_{\parallel} are given. Hyperfine coupling constants were calculated using $\mu(^{231}\text{Pa}) = 2.01 \mu_N$ and $I = 3/2$ [84]. The DC-FSCCSD/dyall.ae4z results were computed at the equilibrium bond length taken from the ZORA-cGKS-B3LYP calculations.

| State | Method | $r_e/\text{\AA}$ | $\tilde{\omega}_e/\text{cm}^{-1}$ | $\tilde{T}_e/\text{cm}^{-1}$ | Λ | $ \bar{\mu} ^2/(e^2 a_0^2)$ | A_{\parallel}/MHz |
|-------------------|----------------------|------------------|-----------------------------------|------------------------------|-----------|-----------------------------|----------------------------|
| (X)5/2 | ZORA-cGHF | 1.87 | 846 | — | 2.9 | — | −983 |
| | ZORA-cGKS-B3LYP | 1.89 | 828 | — | 2.8 | — | −1020 |
| | ZORA-cGKS-PBE0 | 1.87 | 828 | — | 2.8 | — | −1020 |
| | DC-FSCCSD/dyall.ae3z | 1.85 | 859 | — | — | — | — |
| | DC-FSCCSD/ANO-RCC | 1.85 | 892 | — | — | — | — |
| (1)3/2 | ZORA-cGHF | 1.87 | 829 | 1250 | 1.8 | 3×10^{-3} | −953 |
| | ZORA-cGKS-B3LYP | 1.88 | 816 | 152 | 1.9 | 4×10^{-3} | −1140 |
| | ZORA-cGKS-PBE0 | 1.86 | 815 | 185 | 1.9 | 4×10^{-3} | −1130 |
| | DC-FSCCSD/dyall.ae3z | 1.85 | 844 | 658 | — | — | — |
| | DC-FSCCSD/dyall.ae4z | — | — | 752 | — | — | — |
| DC-FSCCSD/ANO-RCC | 1.84 | 876 | 646 | — | — | — | |
| (1)1/2 | ZORA-cGHF | 1.87 | 840 | 3020 | 0.6 | 6×10^{-8} | −1050 |
| | ZORA-cGKS-B3LYP | 1.89 | 831 | 3470 | 0.8 | 2×10^{-9} | −1600 |
| | ZORA-cGKS-PBE0 | 1.87 | 830 | 3540 | 0.8 | 1×10^{-11} | −1560 |
| | DC-FSCCSD/dyall.ae3z | 1.86 | 852 | 3060 | — | — | — |
| | DC-FSCCSD/dyall.ae4z | — | — | 3050 | — | — | — |
| DC-FSCCSD/ANO-RCC | 1.85 | 885 | 2990 | — | — | — | |
| (1)7/2 | ZORA-cGHF | 1.87 | 849 | 5520 | 3.0 | 2×10^{-4} | −328 |
| | DC-FSCCSD/dyall.ae3z | 1.85 | 862 | 5540 | — | — | — |
| | DC-FSCCSD/dyall.ae4z | — | — | 5550 | — | — | — |
| | DC-FSCCSD/ANO-RCC | 1.85 | 895 | 5550 | — | — | — |
| (1)5/2 | ZORA-cGHF | 1.87 | 831 | 6440 | 2.1 | 2×10^{-3} | −329 |
| | DC-FSCCSD/dyall.ae3z | 1.84 | 846 | 5790 | — | — | — |
| | DC-FSCCSD/dyall.ae4z | — | — | 5680 | — | — | — |
| | DC-FSCCSD/ANO-RCC | 1.84 | 878 | 5680 | — | — | — |
| (2)3/2 | ZORA-cGHF | 1.87 | 838 | 8000 | 1.2 | 5×10^{-4} | −329 |
| | DC-FSCCSD/dyall.ae3z | 1.85 | 853 | 7810 | — | — | — |
| | DC-FSCCSD/dyall.ae4z | — | — | 7830 | — | — | — |
| | DC-FSCCSD/ANO-RCC | 1.85 | 885 | 7780 | — | — | — |
| (2)1/2 | ZORA-cGHF | 1.87 | 841 | 8890 | 0.4 | 1×10^{-11} | −473 |
| | DC-FSCCSD/dyall.ae3z | 1.86 | 857 | 8940 | — | — | — |
| | DC-FSCCSD/dyall.ae4z | — | — | 9040 | — | — | — |
| | DC-FSCCSD/ANO-RCC | 1.85 | 890 | 8960 | — | — | — |
| (3)3/2 | ZORA-cGHF | 1.84 | 888 | 30 000 | 2.0 | 0.5 | −2600 |
| | DC-FSCCSD-dyall-ae3z | 1.82 | 882 | 29 200 | — | — | — |
| | DC-FSCCSD/dyall.ae4z | — | — | 29 900 | — | — | — |
| | DC-FSCCSD-ANO-RCC | 1.82 | 901 | 28 900 | — | — | — |

TABLE V. **The transition properties relevant for investigating laser-cooling are shown for the transitions between the eight lowest states of PaF³⁺.** Excitation energies T_e , Einstein coefficients A for spontaneous emission from electronic states (as detailed in the methods section) and Franck–Condon factors for the 0-0 transition ($f^{(0)}$) and cumulated for the 1-0 transition ($f^{(1)}$) are computed on the level of ZORA-cGHF. The life-time of electronic states τ_e is estimated from the electronic Einstein coefficients as $(\sum_a A_i^a)^{-1}$ for each state i , where A_i^a is the Einstein coefficient for the electronic spontaneous emission from i to a . Franck–Condon factors in parantheses indicate that the corresponding vibrational level lies above the vibrational ground state of the next higher electronic state.

| | (1)3/2 | (1)1/2 | (1)7/2 | (1)5/2 | (2)3/2 | (2)1/2 | (3)3/2 |
|------------|--|--|--|--|--|---|--|
| τ_e/s | 7×10^{-2} | 6×10^{-3} | 2×10^{-2} | 7×10^{-4} | 4×10^{-4} | 6×10^{-6} | 2×10^{-8} |
| (X)5/2 | T_e/cm^{-1} 1300 T_e/nm 7700 A/s^{-1} 1×10^1 $f^{(0)}$ 0.9855 $f^{(1)}$ (0.9999) | 3000 3300 3×10^{-3} 0.9856 0.9999 | 5500 1800 5×10^1 0.9994 0.9999 | 6400 1600 1×10^3 0.9844 0.9999 | 8000 1300 5×10^2 0.9989 0.9999 | 8800 1100 2×10^{-5} 0.9999 0.9999 | 30000 300 3×10^7 0.7391 0.9570 |
| (1)3/2 | T_e/cm^{-1} T_e/nm A/s^{-1} $f^{(0)}$ $f^{(1)}$ | 1800 5500 2×10^2 0.9857 0.9997 | 4300 2300 2×10^{-5} 0.9795 0.9994 | 5200 1900 3×10^2 0.9999 0.9999 | 6700 1500 2×10^3 0.9922 0.9999 | 7500 1300 1×10^5 0.9843 0.9997 | 29000 300 1×10^7 0.8342 0.9798 |
| (1)1/2 | T_e/cm^{-1} T_e/nm A/s^{-1} $f^{(0)}$ $f^{(1)}$ | | 2500 4000 5×10^{-7} 0.9994 0.9999 | 3400 2900 3×10^{-4} 0.9846 0.9999 | 5000 2000 1 0.9989 0.9999 | 5800 1700 1×10^4 0.9969 0.9999 | 27000 370 1×10^6 0.7399 0.9563 |
| (1)7/2 | T_e/cm^{-1} T_e/nm A/s^{-1} $f^{(0)}$ $f^{(1)}$ | | | 920 10900 3 0.9782 (0.9999) | 2500 4000 3×10^{-3} 0.9969 0.9999 | 3300 3030 2×10^{-6} 0.9997 0.9999 | 24000 400 9×10^{-2} 0.7194 0.9509 |
| (1)5/2 | T_e/cm^{-1} T_e/nm A/s^{-1} $f^{(0)}$ $f^{(1)}$ | | | | 1600 6300 1×10^2 0.9914 (0.9999) | 2400 4200 2×10^{-6} 0.9831 0.9997 | 24000 400 1×10^6 0.8374 0.9806 |
| (2)3/2 | T_e/cm^{-1} T_e/nm A/s^{-1} $f^{(0)}$ $f^{(1)}$ | | | | | 820 12200 1×10^1 (0.9986) (0.9999) | 22000 500 3×10^5 0.7768 0.9670 |
| (2)1/2 | T_e/cm^{-1} T_e/nm A/s^{-1} $f^{(0)}$ $f^{(1)}$ | | | | | | 21000 500 1×10^3 0.7353 0.9550 |

TABLE VI. \mathcal{P}, \mathcal{T} -odd electronic structure parameters for PaF^{3+} are shown. The properties were calculated on the level of ZORA-cGHF and ZORA-cGKS-B3LYP and PBE0. For computation of the magnetic interaction with the proton EDM $W_m \mu(^{231}\text{Pa}) \simeq 2.01\mu_N$ [84] and $I = 3/2$ were used.

| State | Method | $W_S / \frac{e}{4\pi\epsilon_0 a_0^4}$ | $W_m / \frac{10^{18} \text{ h Hz}}{e \text{ cm}}$ | $W_T / (h \text{ Hz})$ | $W_d / \frac{10^{24} \text{ h Hz}}{e \text{ cm}}$ | $W_s / (h \text{ kHz})$ | $W_{\mathcal{M}} / \frac{10^{33} \text{ h Hz}}{e e \text{ cm}^2}$ |
|--------|-----------------|--|---|------------------------|---|-------------------------|---|
| X5/2 | ZORA-cGHF | -72 000 | 6.3 | -6700 | 0.66 | 4.2 | 0.038 |
| | ZORA-cGKS-B3LYP | -58 000 | 4.9 | -5300 | 0.41 | 2.5 | 0.023 |
| | ZORA-cGKS-PBE0 | -58 000 | 4.9 | -5400 | 0.41 | 2.9 | 0.027 |
| (1)3/2 | ZORA-cGHF | -66 000 | 5.5 | -6200 | 1.4 | 9.3 | -0.022 |
| | ZORA-cGKS-B3LYP | -53 000 | 4.5 | -4900 | 0.92 | 5.8 | -0.0023 |
| | ZORA-cGKS-PBE0 | -54 000 | 4.4 | -5000 | 1.1 | 6.8 | -0.0018 |
| (1)1/2 | ZORA-cGHF | -59 000 | 4.8 | -5600 | 2.9 | 20 | -0.10 |
| | ZORA-cGKS-B3LYP | -49 000 | 4.1 | -4800 | 1.8 | 12 | -0.13 |
| | ZORA-cGKS-PBE0 | -49 000 | 3.9 | -4600 | 2.0 | 13 | -0.14 |
| (1)7/2 | ZORA-cGHF | -73 000 | 6.4 | -6800 | -0.48 | -3.0 | -0.030 |
| (1)5/2 | ZORA-cGHF | -68 000 | 5.7 | -6400 | -0.28 | -1.9 | -0.0014 |
| (2)3/2 | ZORA-cGHF | -61 000 | 5.1 | -5500 | -0.22 | -1.6 | 0.061 |
| (2)1/2 | ZORA-cGHF | -58 000 | 4.9 | -5500 | -0.36 | -2.6 | 0.14 |
| (3)3/2 | ZORA-cGHF | -70 000 | 5.8 | -6600 | 3.2 | 19 | 0.14 |